Tensile strength of axially loaded unidirectional Nextel 610™ reinforced aluminium: a case study in local load sharing between randomly distributed fibres.

A. Rossoll[1], B. Moser[1,2], A. Mortensen[1]

[1] Laboratory of Mechanical Metallurgy, École Polytechnique Fédérale de Lausanne (EPFL), CH-1015 Lausanne, Switzerland.
[2] Now with: Suisse Technology Partners AG, RhyTech Areal, Badische Bahnhofstrasse 16, CH-8212 Neuhausen am Rheinfall, Switzerland.

Keywords: A. Metal-matrix composites (MMCs); B. Strength; C. Statistical properties/methods; D. Mechanical testing.

ABSTRACT

The tensile failure of unidirectional alumina fibre reinforced aluminium is studied in uniaxial loading along the fibre axis. The tensile strength is measured as a function of matrix yield strength, which is varied by varying the testing temperature, from RT to 600 °C. Over the range of matrix yield strength (i.e., of temperature) examined, the fracture mode remains brittle. Batdorf's (J Reinforced Plastics Compos 1982;1:153-164) simple ideal local load–sharing model describes well the observed behaviour, under the condition that it be adapted to account for the actual number of nearest neighbours characteristic of the fibre distribution in the composite. This is shown to be close to three, *i.e.,* at variance with the usually assumed idealized hexagonal or square fibre arrangement patterns.

1. Introduction

Before a composite fails, it nearly always accumulates internal damage [1-6]. Sometimes damage spreads uniformly within the material; it then mostly reduces the

apparent stiffness of the composite, causing tensile deformation to become unstable when the Considere criterion is met if the composite flow stress is independent of the strain-rate. The composite ultimate tensile strength is then reached at a smooth maximum, situated where the composite apparent stiffness has fallen to equal its flow stress (*e.g.,* [7]).

Often, however, composite tensile failure is much more abrupt: under tension, the composite accumulates some internal damage and then breaks suddenly, well before the Considere criterion is met (*e.g.,* [8, 9]). This difference in behaviour is linked with differences in the path of damage accumulation. If damage is uncorrelated, meaning if one damaged site does not promote the formation of more damage in its vicinity, internal damage builds in relatively uniform fashion throughout the material. Graceful failure is then observed when testing under displacement control, the tensile curve showing a smooth maximum if the composite contains many fibres. If damage is, on the other hand, correlated, meaning if a damage event tends mostly to increase the probability for more damage mainly in its immediate surroundings, then a region of concentrated damage can appear and grow through the material. When such growth becomes unstable, an avalanche of internal damage suddenly cuts the material in two, well before most of the material sees much damage.

In a unidirectionally reinforced fibre composite stressed along its fibres, unless the matrix is brittle, internal damage is in the form of individual broken fibres. What then determines the composite fracture mode, and by implication its tensile strength, is the propensity of one broken fibre to cause neighbouring fibres to break. This, in turn, is determined by several parameters, which include the fibre and matrix properties, the strength of the interface, and the geometrical arrangement of fibres in the matrix [1-5, 10-12]. This problem, of load transfer from one broken fibre to other fibres and to the matrix in its vicinity, is complex and has been addressed, for various combinations of matrix, fibre and interfacial strength, by many authors [2, 3, 8, 10, 11, 13-23].

Two limiting cases are often considered, as these give extremes for which the problem is well defined and more tractable [2, 3, 10-12, 24-26]. One is Equal or Global Load Sharing (ELS or GLS), where the load from one broken reinforcement is shed equally to all remaining intact reinforcements across the composite in that section of the composite, roughly one stress-transfer length long, that contains the broken fibre. GLS favours a gradual build-up of dispersed damage within the composite. The other

extreme is local load sharing (LLS). This assumes that a broken fibre sheds all the load it carried before fracture to its immediate neighbours only. LLS clearly favours damage propagation from one broken fibre to its neighbours, making the composite prone to break suddenly. It seems intuitively evident that GLS is favoured by a very weak matrix or fibre/matrix interface, given that this is how a bundle of loose fibres fails. LLS, on the other hand, tends to be favoured in composites that feature a strong interface between fibre and matrix. There are in the literature several spectacular examples of a transition between smooth tensile failure with many debonded fibres to brittle and sudden failure with a flat fracture surface, where the transition is brought about by increasing interface strength, all else (matrix, fibre) equal. Such examples exist in fibre-reinforced ceramic [27], polymer [1, 7, 10, 28] and metal matrix [29] composites.

We present here a study of the longitudinal tensile fracture of a high-strength metal matrix composite made of aluminium reinforced with alumina fibres. This composite was produced in wire form by 3M (St Paul, MN, USA) using an infiltration process, and is used for the overhead transmission of electrical power [30] or the local reinforcement of aluminium castings [31]. We compare theory with experiment in two ways: (i) by direct comparison of strength predicted in the absence of adjustable parameters with experimental data, and (ii) by studying the influence of variations in matrix flow stress. This we accomplish by carrying out the testing at temperatures ranging from room temperature (RT) up to 600 °C. We show that, over the whole range of temperatures (matrix strengths) examined, the simple LLS model proposed by Batdorf [32, 33], which we extend here to relax the low-stress approximation of Weibull statistics, yields a very satisfying description of both the physics of composite fracture and of our data, *provided* realistic assumptions are taken on the microstructure of the composite. That is, instead of assuming a square [10, 13, 19, 20, 22, 34-37] or hexagonal [8, 10, 13, 15, 16, 19, 23, 38-48] fibre arrangement as is nearly always done in 3D fibre composite theory, we consider another idealized fibre arrangement, which is based on results of statistical image analysis on the composite material. As will be seen, the arrangement thus deduced, in which each fibre has only three neighbours, leads to good direct agreement between theory and experiment. It also gives a simple alternative explanation for frequent prior reports in the literature of higher-than-predicted SCF values or lower-than-predicted experimental strength values in composites failing by LLS [10, 11, 40, 44, 47, 49].

2. Experimental procedures

The continuous alumina fibre reinforced pure aluminium matrix composite wire of this work was produced by 3M (St Paul, MN, USA) and was supplied on a reel. The wire contains about 50 vol.% of continuous alumina fibre Nextel 610™ (3M, St Paul, MN, USA). This fibre is composed of >99% α-Al_2O_3 and has a mean UTS of 3380 MPa at L_0 = 25 mm with a Weibull modulus of 11.2 [50, 51]; additional detailed data can be found in Refs. [40, 50-53]. The wire has a roughly circular cross-section with an equivalent diameter of 1.99 mm (determined by volume measurement). 99.9% pure Al is used as the matrix [54]. A micrograph giving a cross sectional view of the composite wire is given in Fig. 1 of Ref. [55]; representative micrographs of its structure taken at a higher magnification are shown in Fig. 1 of the present publication.

Tensile tests were conducted on a computer-controlled Alliance RT/50 (MTS, MN, USA) screw-driven universal testing machine equipped with a 5 kN load cell. The wire sample gauge length was 180 mm. Elevated temperature tests were conducted using an MTS environmental chamber for tests at 100 °C, and using a ZG.19.519-000 Heraeus (Heraeus, Hanau, Germany) resistance tube furnace for temperatures above 100 °C. In elevated temperature tests, the length of the hot zone was also approximately 180 mm, *i.e.,* identical to the gauge length in lower temperature samples. All tests were conducted at a nominal strain rate of 10^{-4} s^{-1}.

The fibre distribution was analyzed in a similar way as that described in Refs. [56, 57] on a polished surface half the cross section of the wire (roughly 7500 fibres). Each micrograph contained typically 130 fully visible fibres (meaning fibres uncut by the picture frame). The distances from a given fibre to its 1st to 6th nearest neighbours were determined as follows: (i) images taken in optical microscopy (768 × 576 pixels in size) were preprocessed by the aid of the *imageJ* software (functions “make binary” and “watershed”, as well as “noise -> remove outliers”) [58]. The size of fibres (in pixels) was computed by the aid of the “analyze particles” function. The “binary -> find maxima” function was used to identify fibre centres. Their coordinates were then used as input to the statistics software “*R*” [59]. Nearest-neighbour distances between fibre centres were computed using the “nndist” function provided in the “spatstat” package [60], and

converted to surface-to-surface distances knowing the fibre diameter. This is justified under condition that the fibre diameter distribution be roughly monomodal, a condition that is fulfilled here exception made for a few significantly smaller fibres that were occasionally encountered; these were discarded from analysis.

3. Experimental results

Figure 2 gives the distribution of measured distances from random fibres to their 1st to 6th nearest neighbours. It can be seen that the fibre distance increases continuously from the 1st to the 6th nearest neighbours—which is reassuring of course, but also shows that there is no well-defined ring of nearest neighbours surrounding each fibre within the composite, as is generally assumed in models. Almost all (90%) of the fibres have at least one neighbour in their immediate vicinity, *i.e.,* in direct or nearly direct touching contact; this is immediately visible in Fig. 1. Many fibres have several such directly contacting neighbours; their number decreases steadily down to roughly 4. The likelihood of immediate contact with the 4th neighbour is small (roughly 10%) while the probability of a fibre contacting 5 neighbours is almost nil. Taking as a definition for contact or near-contact a measured distance between two fibres that is less than 10% of their radius (0 to 2 μm), one concludes that most fibres touch or nearly touch about 2–3 neighbours, something that is confirmed by close examination of the micrographs shown in Fig. 1.

The shape of the composite tensile curves is almost linear, with slight nonlinearity arising both from matrix plasticity and from non-linear elastic deformation of the fibres [54, 61]. A change in slope due to fibre damage may be expected, notably shortly before failure when the damage growth rate is highest (as suggested from acoustic emission experiments [9]); however, no pronounced slope change could be detected on the recorded load-displacement curves over the range of test temperatures examined. Clearly the amount of damage accumulated prior to fracture is not sufficient to induce tensile instability, Fig. 3.

SEM images of fracture surfaces of wires tested at room temperature and at 600 °C are shown in Figs. 4a and b, respectively: apart from regions of fibre pull–out betraying a softer matrix at 600 °C, fracture surfaces look similar. Large portions on both fracture

surfaces are flat and indicate a brittle failure mode, consistent with the observed shape of load–displacement curves.

The composite wire has a mean strength of 1380 MPa (±40 MPa standard deviation) at room temperature. Its ultimate tensile strength decreases monotonically with increasing temperature in the range from 20 °C to 600 °C, as shown in Fig. 5. We note in passing that above the matrix melting temperature (660 °C), the composite strength drops sharply and becomes a strong function of the molten length; such data are given in an earlier study where this technique was used to measure damage accumulation within the composite [55].

Also noteworthy is the fact that no transition towards GLS behaviour is found with matrix softening, betraying a strong prevalence of LLS in this material. This is not necessarily the case for other systems. For instance, a transition was observed in Fuwa *et al.*'s semi–cured organic matrix composites [28] and Hauert *et al.*'s particle reinforced aluminium [62, 63], and was demonstrated in a planar LLS model by Phoenix and Newman [64].

4. Theory

In LLS, composite fracture is caused by the formation of a (often complex and statistically variable) critical cluster containing a limited number of fractured fibres that propagates catastrophically above a certain stress; the ensuing fibre fracture "avalanche" then abruptly breaks the composite. This cluster forms starting from a single fibre fracture which, as stress increases, causes successive failure in nearby fibres. This in turn occurs because of the increased stress the broken fibre induces in its neighbours over a length roughly equal to 2δ, where the stress transfer length δ is taken as half the critical length [65] given by

$$\delta = \frac{\sigma_{\mathrm{f}} \cdot r_{\mathrm{f}}}{2 \cdot \tau_{\mathrm{y,m}}} \tag{1}$$

where σ_{f} is the fibre remote stress, r_{f} is the fibre radius and $\tau_{\mathrm{y,m}}$ the matrix shear yield stress.

Batdorf proposed a simplified yet comparatively clear framework for analysis of such composite fracture behaviour, which has been shown to be fairly accurate for relatively large values of the fibre Weibull modulus m (defined immediately below), such values being typical of high-quality ceramic fibres [18]. We use it hereafter essentially as it was originally formulated [2, 18, 32, 33], but adapt it to incorporate the full expression for fibre Weibull failure probability:

$$P = 1 - \exp\left[-\frac{L}{L_0} \cdot \left(\frac{\sigma_\mathrm{f}}{\sigma_0} \right)^m \right] \tag{2}$$

instead of the first order approximation used by Batdorf, which can lose validity in the present context. In Eq. (4), L is the length of the fibre, L_0 the Weibull reference length, σ_0 the Weibull reference stress, and m the Weibull modulus. This introduces no great complication to the derivation while making some of its points clearer.

Consider a composite specimen containing N fibres, all of length B, subjected to tensile stress σ parallel to the fibres, which represent a volume fraction V_f of the composite volume. The matrix surrounding the fibres has a shear yield strength $\tau_{\mathrm{y,m}}$. If we ignore work hardening of the matrix (a legitimate assumption in the present composites [54]), then the fibre stress σ_f can be calculated from the equistrain rule of mixtures, known to be valid in this configuration:

$$\sigma = V_\mathrm{f} \cdot \sigma_\mathrm{f} + \left(1 - V_\mathrm{f}\right) \cdot M \cdot \tau_{\mathrm{y,m}} \tag{3}$$

where $M = \sqrt{3}$ is the (von Mises) conversion factor from shear to tensile yield stress.

To calculate the number of uncorrelated single fibre breaks ("singlets") we account for the possibility of multiple fracture of each fibre provided breaks are one transfer length δ apart. The number of singlets Q_1 created at given σ_f, is therefore

$$Q_1 = N \cdot \frac{B}{2 \cdot \delta} \cdot \left[1 - \exp\left(-\frac{2 \cdot \delta}{L_0} \cdot \left(\frac{\sigma_\mathrm{f}}{\sigma_0} \right)^m \right) \right]. \tag{4}$$

If an isolated fibre break causes fracture of one neighbouring fibre, the result is the formation of a pair of correlated fibre breaks (a doublet). If this doublet in turn causes fracture in another neighbouring fibre, a triplet is formed, and so on to form i neighbouring fibre breaks, resulting in a cluster of broken fibres called an "i-plet". Rules for damage propagation can vary; a fairly elaborate example is given by Smith *et al*. [66]. The Batdorf model simplifies the complex statistical problem of fracture propagation in fibre composites by assuming that, around each cluster of i broken fibres, the stress concentration in the corresponding n_i nearest neighbouring fibres is uniform. The Stress Concentration Factor (SCF) is then

$$s_i = \frac{\sigma_{\max,i}}{\sigma_\mathrm{f}} = 1 + \frac{i}{n_i} \tag{5}$$

where $\sigma_{\max,i}$ is the maximum stress on fibres neighbouring an i-plet, in a composite with a given (far field) fibre stress σ_f. Fibres more distant from a broken fibre cluster than its nearest neighbours are on the other hand assumed to experience no stress concentration, the fibre stress thus being σ_f there (the model thus assumes perfectly localized load sharing).

The overload on a fibre neighbouring a broken fibre is approximated by Batdorf as a triangular stress profile along the fibre axis. The peak value, $\sigma_\mathrm{f}\ s_i$, is reached in the fracture plane and the far field fibre stress σ_f is again reached at a distance δ away from the fracture plane in either direction. This stress profile can be replaced by a constant stress concentration s_i acting over a length λ_i that is defined such that the resulting Weibull failure probability of the fibre be the same as for the triangular profile; the result is [32]:

$$\lambda_i = 2 \cdot \delta \cdot \frac{s_i^{m+1} - 1}{s_i^m \cdot \left(s_i - 1\right) \cdot \left(m + 1\right)}. \tag{6}$$

The local failure probability for overloaded fibres neighbouring an i-plet is thus

$$P_{\text{overloaded}} = 1 - \exp\left(-\frac{\lambda_i}{L_0} \cdot \left(\frac{s_i \cdot \sigma_{\text{f}}}{\sigma_0} \right)^m \right). \tag{7}$$

The probability that a singlet transform into a doublet (by breaking one of its neighbours) is then calculated knowing that the total overloaded length is λ_1 times the number of nearest neighbours n_1

$$P_{1\to 2} = 1 - \exp\left(-\frac{n_1 \cdot \lambda_1}{L_0} \cdot \left(\frac{s_1 \cdot \sigma_{\text{f}}}{\sigma_0} \right)^m \right). \tag{8}$$

The number of doublets formed by this process in the composite is then simply $Q_2 = Q_1 \cdot P_{1\to 2}$. Similarly, the number of *i*-plets created from (*i*-1)-plets is $Q_i = Q_{i-1} P_{(i-1)\to i}$. By recursion:

$$Q_i = Q_1 \cdot \prod_{j=1}^{i-1} \left[1 - \exp\left(-\frac{n_j \cdot \lambda_j}{L_0} \cdot \left(\frac{s_j \cdot \sigma_{\text{f}}}{\sigma_0} \right)^m \right) \right]. \tag{9}$$

Equation (9) represents a family of curves if the number of *i*-plets in the composite is plotted as a function of the applied fibre stress for different values of *i*; Fig. 6 gives examples for the present system (parameter values are detailed below).

As *i* increases, s_{i} increases (and λ_i decreases). Indeed, there are fewer neighbouring fibres per broken fibre around a larger cluster than around a smaller cluster. Therefore, fibre fracture propagation is increasingly likely around *i*-plets as *i* increases. Thus, as *i* increases, Q_i tends to stabilize onto a single "high-*i*" master curve. Note that this behaviour differs from that found in Batdorf's original derivation, where having simplified the Weibull statistics to the low-stress limiting expression, Q_i lines were straight and intersected (such that above a certain threshold, which has on occasion later been interpreted as an instability, *i*-plets became more probable as *i* increased—an obviously artificial result). Note the similarity of these curves showing Eq. (9) with the "characteristic distribution function" *W* that was introduced by D.G. Harlow and S.L. Phoenix [25] and extended to 3-D by Smith *et al*. [66] (for comparison, Eq. (9) has to be divided by

$N \cdot B$ / $2 \cdot \delta$). Smith *et al*. also gave an estimate of the limiting curve to which this family of curves converges. Note also that the decrease of λ_i with i also favours the development of a single dominant crack in the specimen, notably for fibres having a high value of m.

Now for each i, the σ_f value at which Q_i equals unity is that at which there is, on average, one i-plet in the composite. The σ_f value at which the asymptotically bundled high-i curves reach unity is thus a σ_f value for which there is on average one cluster that is indefinitely large, or in other words sufficiently large to cut across the composite. The corresponding far-field fibre stress, σ_f^*, is therefore the average fibre stress for which the composite will fracture. The average composite tensile strength σ^* is obtained by substituting σ_f^* into Eq. (3).

In order to compute the stress concentration factors s_i an assumption has to be made on the fibre arrangement. As indicated above, square or hexagonal lattices are nearly always assumed. In a hexagonal arrangement, for example, the number of nearest neighbours for the singlet and doublet is six. This yields 1.17 for s_1; for a doublet the number is eight, and s_2 therefore should equal 1.25, if Batdorf's assumption of uniform SCFs over all the nearest neighbours is maintained. In reality, two of the nearest neighbours bear a higher overload as compared to the others [66]. For a triplet and higher order multiplets the number of nearest neighbours and resulting s_i values depend on the configuration of the i-plet,. Smith *et al.* [66] investigated several scenarios and identified "dominant failure configurations" yielding the largest SCFs. A complication may then arise, however, from the fact that these SCFs do not always increase monotonically with the size of the i-plet. Further investigations were carried out by Mahesh *et al.*, who investigated the influence of the Weibull shape parameter m on the sequence of fibre failures and resulting SCFs for the case of an elastic matrix [38]. In this work we stay with Batdorf's assumption of uniform SCFs over the nearest neighbours, emphasizing however that this is for no better reason than simplicity. Resulting SCFs increase monotonically and are largest for clusters that resemble circles, as these result in the lowest number of nearest neighbours possible for an i-plet of given size; this configuration was thus (conservatively) assumed here in calculating SCFs for each value if i.

Now, as seen above, the actual fibre arrangement in the present aluminium/alumina fibre composite is quite far from being square or hexagonal. We have seen that the number of nearest neighbours to a single fibre is much closer to three than to six and that, on the other hand, the distance to these closest neighbours is typically near zero.

Figure 7 shows a synthetic regular fibre arrangement that has both of these characteristics: it is derived from a regular hexagonal fibre arrangement by simply removing one fibre out of three. Furthermore, when the fibres touch, as drawn in Fig. 7, V_f is 60.46%, which is a realistic value for composite such as that of this work, Fig. 1. We thus take this simple pattern as a basis to compute more realistic numbers for n_i than are obtained from regular square or hexagonal fibre packings. Resulting values are given in Table 1, together with those resulting from the assumption of a regular hexagonal fibre arrangement.

From a mean fibre strength of 3380 MPa and knowing m = 11.2 [50, 51] it follows that σ_0 = 3490 MPa for L_0 = 25 mm (at room temperature). To assess the *in-situ* matrix properties, necessary for computing the stress transfer length and known to differ from bulk properties due to the presence of geometrically necessary dislocations in the metal, we make use of the data given in Ref. [54]. These values were obtained by "back-calculating" the matrix flow stress from composite tensile tests conducted at room temperature (note that the solution of this inverse problem requires a very high precision, since the sought-after results corresponds to the difference of two large numbers, namely the composite and fibre stress, respectively). This gives the room-temperature values of $\tau_{y,m}$. Corresponding curves of Q_i versus σ_f are given in Fig. 6, for fibre packings featuring three or six neighbours.

The required precision is difficult to obtain when testing at elevated temperature, which is why for elevated temperature we use literature data to evaluate $\tau_{y,m}$. The matrix material is nominally pure aluminium but contains traces of iron and silicon, which increase the metal flow stress, notably at elevated temperature [54, 67]. The high density of geometrically necessary dislocations present from cooldown from processing temperature is also expected to induce a strain rate sensitivity in tensile loading that is more characteristic of steady state creep rather than primary creep, even at low applied mechanical strain. Based on this reasoning and on data plotted in Fig. 5 of Ref. [67], we estimate $\sigma_{y,m} = M\,\tau_{y,m}$ at elevated temperature as given in Table 2. For each temperature, we also give the corresponding stress transfer length δ (Eq. 1).

For completeness, we compare our data also with a GLS model. Curtin developed an elegant statistical shear-lag analysis yielding a simple prediction for the tensile strength of a fibre composite under global load sharing conditions [11, 27, 68, 69]. Failure occurs

through geometrical instability (zero slope in the stress-strain curve). The predicted composite strength is then

$$\sigma_{\mathrm{UTS}} = V_{\mathrm{f}} \cdot \sigma_{\mathrm{c}} \cdot \left(\frac{2}{m+2} \right)^{\frac{1}{m+1}} \cdot \left(\frac{m+1}{m+2} \right) + \left(1 - V_{\mathrm{f}}\right) \cdot \sigma_{\mathrm{y,m}} \tag{10}$$

where σ_{c} is defined as

$$\sigma_{\mathrm{c}} = \left(\frac{\sigma_0^m \cdot \tau_{\mathrm{y,m}} \cdot L_0}{r_{\mathrm{f}}} \right)^{\frac{1}{m+1}} \tag{11}$$

and depends on the statistical fibre properties (via the fibre diameter, r_{f}, characteristic stress and length values, σ_0 and L_0, respectively, and the Weibull modulus m) and the shear yield strength of the matrix, $\tau_{\mathrm{y,m}}$.

5. Discussion

LLS (treating both six and three neighbour fibre packing configurations) and GLS predictions of composite strength are plotted in Fig. 5 together with our experimental data. The GLS and both LLS models all capture well the experimentally observed trend of decreasing composite strength with increasing temperature. This is because the influence of this parameter is common to all three models, namely a reduced matrix flow stress has as its main consequence an increased δ, leading in turn to an increased probability for fibre fracture following fracture of another fibre, Eqs. (1), (6) and (7). This influence is relatively weak, due to the elevated value of the Weibull shape parameter of the present fibres. An uncertainty in $\tau_{y,m}$ therefore translates only weakly as an uncertainty in the composite fracture stress. This can immediately be seen on Fig. 5: a decrease of $\tau_{y,m}$ by one order of magnitude (as encountered by a change of test temperature from room temperature to 400 °C, see Table 2) induces a drop in composite strength of only about 16%.

On the other hand, of the three models only the LLS model with three direct neighbours to a single fibre yields a good overall description of experimental data (note that there are no adjustable parameters used in the comparison). This agrees with

general features of fracture in the present composite: the sudden load drop on tensile curves, Fig. 3, and the shape of fracture surfaces showing large portions of coplanar fibre cracks, Figs. 4 a and b, clearly indicate a prevalence of LLS.

The only notable discrepancy is at the highest testing temperature, 600 °C, where experimental values fall roughly 10% below those computed. This may be because at that temperature the fibre strength starts to degrade. For elevated temperatures just below 800 °C, no results on the fracture strength of Nextel 610™ seem to be available in the literature; however, it has been established that at 800 °C the fibre fracture strength is much lower than at room temperature [51]. It thus seems plausible that creep already reduce the fibre strength at 600°C, which might explain that experimental values lie below those predicted here on the basis of a constant fibre strength.

The role of LLS on composite failure and associated size effects follow also from the scatter of the composite fracture stress, although the number of samples is not sufficient to obtain reliable data. If we nonetheless attempt to determine the Weibull modulus from our samples (we use a predictor of (i-0.5)/N and linear regression analysis as in [51]), we obtain (bias-corrected) values of 32 (from 7 samples), of 116 (from a mere 3 samples), of 24 (from 7 samples), 100 (from 5 samples) and 46 (from 7 samples), for the samples tested at temperatures of 23 °C, 100 °C, 400 °C, 500 °C and 600 °C, respectively. Given the fact that the number of samples available is so small (95% confidence intervals for a population of 10 samples are fairly large with about 0.5 $m < m_{\text{true}} < 1.9\ m$ [70]; these are of course even larger for the present even smaller sample populations), this large scatter of values of the Weibull modulus is not surprising. Still, the above values suggest that the "true" Weibull modulus of the composite samples is high, and lies probably around 50, which corresponds to $i \cdot m$, as expected for LLS. Now, if we plot Fig. 6a (Q_i as a function of fibre stress) as $\ln\ln(1/(1- Q_i)$ vs. $\ln(\sigma_f)$, we indeed obtain Weibull-shaped slopes, with a value for the critical Q_5 curve of 71, *i.e.,* again of a comparable magnitude (but rather on the upper end), Fig. 8. Given the fact that the size of critical i-plets decreases with the number of nearest neighbours considered in the fibre arrangement, this suggests that the relevant number of nearest neighbours may be a bit below 3, say somewhere between 2 and 3, as also suggested from image analysis, Fig. 2.

We note also that, whereas in the present work we chose to better account for the actual fibre packing but stay with uniform SCFs as did Batdorf, another possible approach is that of Smith *et al.* who studied worst-case SCFs for "dominant failure configurations" in a perfect hexagonal fibre array [66]. These SCFs are much higher than

uniform values and of similar magnitude as our "3 nearest neighbours" SCFs (but do not increase monotonically, as already stated). It is likely that the model by Smith *et al*. yield similar results for our material as our "fibre-packing corrected" Batdorf model; however, we also note that it entails is a significantly more involved calculation.

The general conclusion of this work is that it is important to describe the fibre packing and resulting SCFs realistically before explaining how a fibre composite breaks under uniaxial tension; this is in line with calculations of Landis and McMeeking, who studied the effect of eccentricity of a single fibre within a regular (square) arrangement and showed that the increase of the resulting SCF with eccentricity is substantial for both an elastic as well as a plastic matrix or a sliding interface, suggesting in turn that there is a strongly reduced shear coupling with increased fibre spacing, such that the closest neighbours must bear the brunt of load transfer [20]. Fibre distributions vary: monofilaments in a diffusion-bonded SiC/Ti composite are, for example, packed quite regularly as a result of their processing route (*e.g.,* [8, 71]). Being infiltrated, the present composites contain fibres that are on the other hand irregularly distributed and that often touch, and as such resemble fibre packings found in polymer matrix composites (*e.g.,* Fig. 3.3 of Ref. [1] or Fig. 5.10 of Ref. [72]) or some ceramic matrix composites (*e.g.,* Fig. 7.2 of Ref. [72])—it would be interesting to test whether the present simple three-neighbour model gives a better description of the longitudinal tensile strength of such composites as well. It is also interesting to note that fibre distributions can be engineered to optimize the strength of composites: this was elegantly demonstrated in "hybrid" fibre reinforced metals, where ceramic particles are placed along the fibre surface to keep these apart during composite processing [73-76]: higher longitudinal tensile strengths are indeed obtained.

Another interesting question is the extent to which direct fibre–fibre contact contributes to enhance overloading in the vicinity of fibre breaks via fibre-to-fibre friction: the friction coefficient of alumina is fairly high, around 0.4–0.6 over the range of temperatures examined in our study [77], and the transverse stress state across the matrix cross section is compressive both after cooldown from processing temperature and in tensile loading. This stress state therefore tends to squeeze the fibres against each other, such that substantial friction stresses may develop along the fibre axis. A parallel can be drawn with observations made in composites having organic matrices and reinforced with carbon or glass fibres. These composites exhibit a drop of strength

under tensile loading with increasing superposed hydrostatic pressure, which is accompanied by an increasing flatness of fracture surfaces [78-80]. The authors explain this observation as an effect of the compressive stress normal to the fibre–matrix interface, which impedes fibre pull-out and thus embrittles the composite. Finally we note that a more efficient stress transfer from a broken fibre to its neighbours may also arise from dynamic loading effects as well as from local matrix hardening in regions of small fibre spacing.

6. Concluding remarks

Over the entire range of temperatures (matrix strength values) explored, failure in high-performance infiltrated alumina fibre reinforced aluminium is clearly dominated by LLS. The classical assumption of a hexagonal fibre arrangement fails to provide a satisfying prediction of experimental data. We rationalize this observation through the fact that the actual fibre distribution in the composite is such that each fibre has typically about 2–3 nearest neighbours instead of 6 as commonly assumed. We consider a still idealized but more representative fibre arrangement pattern, where each fibre has three direct neighbours, which together with Batdorf's simple LLS model enables a very satisfying prediction of experimental results across the range of temperatures explored here.

From the above we can deduce that the present composites can likely be made stronger by (i) increasing the matrix strength (free of any embrittling phases however), and (ii) by assuring a more regular fibre distribution designed to increase the number of immediate fibre neighbours and to prevent fibre–fibre contact.

Acknowledgements

This work was funded by a joint EMPA/EPFL PhD thesis program and by internal funding of the Laboratory of Mechanical Metallurgy at EPFL. The authors would like to thank the 3M company for the donation of the composite wire used throughout this study and Dr. Colin McCullough (3M company) for many stimulating discussions. We

would also like to acknowledge the pertinent comments of two unknown referees who have contributed to improve the paper.

References

[1] Hull D, Clyne TW. Introduction to Composite Materials, Second Edition. Cambridge, U.K.: Cambridge University Press; 1996.

[2] Curtin WA. Stochastic damage evolution and failure in fiber-reinforced composites. Adv Appl Mech. 1999;36:163-253.

[3] Phoenix SL, Beyerlein I. Statistical strength theory for fibrous composite materials. In: Kelly A, Zweben C, editors. Comprehensive Composite Materials. Oxford UK: Pergamon; 2000. p. 559-639.

[4] McCartney LN, Broughton WR. Continuous parallel fiber composites: deformation and strength. In: Mortensen A, editor. Concise Encyclopedia of Composite Materials - 2nd Edition. Amsterdam: Elsevier; 2007. p. 255-64.

[5] Blassiau S, Thionnet A, Bunsell AR. Three-dimensional analysis of load transfer micro-mechanisms in fibre/matrix composites. Compos Sci Technol. 2009;69:33-9.

[6] Mishnaevsky Jr L, Br¯ndsted P. Micromechanical modeling of damage and fracture of unidirectional fiber reinforced composites: A review. Comput Mater Sci. 2009;44(4):1351-9.

[7] Huang W, Nie X, Xia Y. Effects of heat-treatment and strain rate on the mechanical properties of SiC/Al composite wires--experimental and constitutive modeling. Compos A. 2005;36(9):1316-22.

[8] González C, Llorca J. Micromechanical modelling of deformation and failure in Ti-6Al-4V/SiC composites. Acta Mater. 2001;49(17):3505.

[9] Rossoll A, Otto C, Moser B, Weber L, Wanner A, Mortensen A. Measurement of damage evolution in continuous ceramic fibre-reinforced metals by acoustic emission. Scripta Mater. 2008;59:842-5.

[10] Wisnom MR, Green D. Tensile failure due to interaction between fibre breaks. Compos. 1995;26:499-508.

[11] Zok FW. Chapter 3.08 - Fracture and fatigue of continuous fiber reinforced metal matrix composites. In: Clyne TW, editor. Comprehensive Composite Materials, Vol 3: Metal Matrix Composites. Oxford UK: Pergamon; 2000. p. 189-220.

[12] Pradhan S, Hansen A, Chakrabarti BK. Failure processes in elastic fiber bundles. Rev Mod Phys. 2010;82:499-555.

[13] Hedgepeth JM, Van Dyke P. Local stress concentrations in imperfect filamentary composite materials. J Compos Mater. 1967;1:294-309.

[14] He MY, Evans AG, Curtin WA. The ultimate tensile strength of metal and ceramic matrix composites. Acta Metall Mater. 1993;41(3):871-8.

[15] Nedele MR, Wisnom MR. Stress concentration factors around a broken fibre in a unidirectional carbon fibre-reinforced epoxy. Compos. 1994;25(7):549-57.

[16] Nedele MR, Wisnom MR. Three-dimensional finite element analysis of the stress concentration at a single fibre break. Compos Sci Technol. 1994;51:517-24.

[17] Ibnabdeljalil M, Curtin WA. Strength and reliability of fiber-reinforced composites: Localized load-sharing and associated size effects. Int J Solids Struct. 1997;34:2649-68.

[18] Foster GC, Ibnabdeljalil M, Curtin WA. Tensile strength of titanium matrix composites: direct numerical simulations and analytic models. Int J Solids Struct. 1998;35(19):2523.

[19] Curtin WA, Takeda N. Tensile strength of fiber-reinforced composites: I. Model and effects of local fiber geometry. J Compos Mater. 1998;32:2042-59

[20] Landis CM, McMeeking RM. Stress concentrations in composites with interface sliding, matrix stiffness and uneven fiber spacing using shear lag theory. Int J Solids Struct. 1999;36(28):4333-61.

[21] Landis CM, McMeeking RM. A shear-lag model for a broken fiber embedded in a composite with a ductile matrix. Compos Sci Technol. 1999;59:447-57.

[22] Landis CM, McGlockton MA, McMeeking RM. An improved shear lag model for broken fibers in composite materials. J Compos Mater. 1999;33:667-80.

[23] Mahesh S, Beyerlein IJ, Phoenix SL. Size and heterogeneity effects on the strength of fibrous composites. Physica D. 1999;133:371-89.

[24] Harlow DG, Phoenix SL. Chain-of-bundles probability model for strength of fibrous materials. 1. Analysis and conjectures. J Compos Mater. 1978;12:195-214.

[25] Harlow DG, Phoenix SL. Chain-of-bundles probability model for strength of fibrous materials. II. A numerical study on convergence. J Compos Mater. 1978(12):314-34.

[26] Hemmer PC, Hansen A, Pradhan S. Rupture processes in fibre bundle models. In: Bhattacharyya P, Chakrabarti B, editors. Modelling Critical and Catastrophic Phenomena in Geoscience: Springer Berlin / Heidelberg; 2006. p. 27-55.
[27] Curtin WA. Theory of mechanical properties of ceramic-matrix composites. J Am Ceram Soc. 1991;74:2837-45.
[28] Fuwa M, Bunsell AR, Harris B. Tensile failure mechanisms in carbon fibre reinforced plastics. J Mater Sci. 1975;10:2062-70.
[29] McCullough C, Deve HE, Channel TE. Mechanical response of continuous fiber-reinforced Al_2O_3-Al composites produced by pressure infiltration casting. Mater Sci Eng. 1994;A189:147-54.
[30] Mortensen A, Llorca J. Metal Matrix Composites. Ann Rev Mater Res. 2010;40:243-70.
[31] Zhang W, Zhang M, Ochiai S, Gu M. Experimental and simulation investigations of tensile response of (Al2O3f/Al)w/2024Al composite. Mater Sci Eng A. 2008;497(1-2):44-50.
[32] Batdorf SB. Tensile strength of unidirectionally reinforced composites – I. J Reinforced Plastics Compos. 1982;1:153-64.
[33] Batdorf SB, Ghaffarian R. Tensile strength of unidirectionally reinforced composites — II. J Reinforced Plastics Compos. 1982;1:165-76.
[34] Zhou SJ, Curtin WA. Failure of fiber composites: a lattice Green function model. Acta Metall Mater. 1995;43(8):3093-104.
[35] Landis CM, Beyerlein IJ, McMeeking RM. Micromechanical simulation of the failure of fiber reinforced composites. J Mech Phys Solids. 2000;48(3):621-48.
[36] Okabe T, Takeda N, Kamoshida Y, Shimizu M, Curtin WA. A 3D shear-lag model considering micro-damage and statistical strength prediction of unidirectional fiber-reinforced composites. Compos Sci Technol. 2001;61(12):1773-87.
[37] Bunsell AR, Thionnet A. Life prediction for carbon fibre filament wound composite structures. Phil Mag. 2010;90(31):4129-46.
[38] Mahesh S, Phoenix SL, Beyerlein IJ. Strength distributions and size effects for 2D and 3D composites with Weibull fibers in an elastic matrix. Int J Fract. 2002;115:41-85.
[39] Xia Z, Curtin WA, Peters PWM. Multiscale modeling of failure in metal matrix composites. Acta Mater. 2001;49(2):273-87.

[40] Xia ZH, Curtin WA. Multiscale modeling of damage and failure in aluminum-matrix composites. Compos Sci Technol. 2001;61(15):2247.
[41] Xia Z, Curtin WA, Okabe T. Green's function vs. shear-lag models of damage and failure in fiber composites. Compos Sci Technol. 2002;62(10-11):1279.
[42] Xia Z, Okabe T, Curtin WA. Shear-lag versus finite element models for stress transfer in fiber-reinforced composites. Compos Sci Technol. 2002;62(9):1141-49.
[43] Okabe T, Takeda N. Elastoplastic shear-lag analysis of single-fiber composites and strength prediction of unidirectional multi-fiber composites. Compos A. 2002;33(10):1327.
[44] Okabe T, Takeda N. Size effect on tensile strength of unidirectional CFRP composites-- experiment and simulation. Compos Sci Technol. 2002;62(15):2053.
[45] Ohno N, Okabe S, Okabe T. Stress concentrations near a fiber break in unidirectional composites with interfacial slip and matrix yielding. Int J Solids Struct. 2004;41(16-17):4263.
[46] Okabe T, Sekine H, Ishii K, Nishikawa M, Takeda N. Numerical method for failure simulation of unidirectional fiber-reinforced composites with spring element model. Compos Sci Technol. 2005;65:921-33.
[47] Okabe T, Nishikawa M, Takeda N, Sekine H. Effect of matrix hardening on the tensile strength of alumina fiber-reinforced aluminum matrix composites. Acta Mater. 2006;54(9):2557-66.
[48] Yuan H, Wen W, Cui H, Xu Y. The random crack core model for predicting the longitudinal tensile strengths of unidirectional composites. J Mater Sci. 2009;44:3026-34.
[49] He J, Beyerlein IJ, Clarke DR. Load transfer from broken fibers in continuous fiber Al2O3-Al composites and dependence on local volume fraction. J Mech Phys Solids. 1999;47:465-502.
[50] Bunsell AR, Berger M-H. Fine diameter ceramic fibres. J Eur Ceram Soc. 2000;20:2249-60.
[51] Wilson DM, Visser LR. High performance oxide Fibers for metal and ceramic composites. Compos A. 2001;32:1143-53.
[52] Wilson DM. Statistical tensile strength of Nextel™ 610 and Nextel™ 720 fibres. J Mater Sci. 1997;32:2535-42.

[53] 3M. NextelTM Ceramic Textiles. Technical Notebook, St Paul, MN, USA, available from: http://www.3m.com/market/industrial/ceramics/misc/tech_notebook.html. 2002.

[54] Rossoll A, Moser B, Weber L, Mortensen A. In situ flow stress of pure aluminium constrained by tightly packed aluminium fibres. Acta Mater. 2009;57:1795-812.

[55] Moser B, Rossoll A, Weber L, Beffort O, Mortensen A. Damage evolution of Nextel 610TM alumina fibre reinforced aluminium. Acta Mater. 2004;52:573-81.

[56] Li QF, McCartney DG, Loh NL. Measurements on fibre distribution in a fibre-reinforced Al Metal-matrix composite (MMC) (matrix intercept-length measurements). J Mater Proc Technol. 1995;51:244-54.

[57] Liu H-N, Ogi K, Miyahara H. The fibre distribution of Al2O3/Al-Cu alloy composites. J Mater Sci. 1998;33:3615-22.

[58] ImageJ. Image Processing and Analysis in Java (http://rsbweb.nih.gov/ij/).

[59] The R Project for Statistical Computing (http://www.r-project.org/).

[60] Baddeley A, Turner R. Spatstat: an R package for analyzing spatial point patterns. J Stat Soft. 2005;12:1-42.

[61] Moser B, Rossoll A, Weber L, Beffort O, Mortensen A. Nextel™ 610 alumina fibre reinforced aluminium: influence of matrix and process on flow stress. Compos A. 2001;32:1067-75.

[62] Hauert A, Rossoll A, Mortensen A. Ductile-to-brittle transition in tensile failure of particle reinforced metals. J Mech Phys Solids. 2009;57:473-99.

[63] Hauert A, Rossoll A, Mortensen A. Particle fracture in high volume fraction ceramic reinforced metals: governing parameters and implications for composite failure. J Mech Phys Solids. 2009;57:1781-800.

[64] Phoenix SL, Newman WI. Time-dependent fiber bundles with local load sharing. II. General Weibull fibers. Phys Rev E. 2009;80:066115-1 -- -13.

[65] Kelly A, Tyson WR. Tensile properties of fibre-reinforced metals - copper/tungsten and copper/molybdenum. J Mech Phys Solids. 1965;13:329-50.

[66] Smith RL, Phoenix SL, Greenfield MR, Henstenburg RB, Pitt RE. Lower-Tail Approximations for the Probability of Failure of Three- Dimensional Fibrous Composites with Hexagonal Geometry. Proceedings of The Royal Society of London Series A, Mathematical and Physical Sciences. 1983;A 388:353-91.

[67] Sherby OD, Goldberg A, Ruano OA. Solute-diffusion-controlled dislocation creep in pure aluminium containing 0.026 at.% Fe. Phil Mag. 2004;84(23):2417-34.
[68] Curtin WA. Ultimate strengths of fibre-reinforced ceramics and metals. Compos. 1993;24:98-102.
[69] Curtin WA, Ahn BK, Takeda N. Modeling brittle and tough stress-strain behavior in unidirectional ceramic matrix composites. Acta Mater. 1998;46:3409-20.
[70] Gong J. Determining the confidence intervals for Weibull estimators. Journal of Materials Science Letters. 1999;18:1405-7.
[71] Weber CH, Chen X, Connell SJ, Zok FW. On the tensile properties of a fiber reinforced titanium matrix composite–I. Unnotched behavior. Acta Metall Mater. 1994;42:3443-50.
[72] Chawla KK. Composite Materials, Science and Engineering - Second Edition. New York: Springer Verlag; 1998.
[73] Yamada S-I, Towata S-I, Ikuno H. Mechanical properties of aluminum alloys reinforced with continuous fibers and dispersoids. In: Fishman SG, Dhingra AK, editors. International Symposium on Advances in Cast Reinforced Metal Composites. Chicago, Illinois, USA: ASM International; 1988. p. 109-14.
[74] Asano K, Yoneda H. Effects of particle-dispersion on the strength of an alumina-reinforced aluminum alloy matrix composite. Mater Trans JIM. 2003;44:1172-80.
[75] Ochiai S, Matsunaga K, Waku Y, Yamamura T, Hojo M, Osamura K. Temperature-dependence mechanism of tensile strength of Si-Ti-C-O fiber-aluminum matrix composites. Metall Mater Trans A. 1995;26A:647-52.
[76] Towata S-I, Ikuno H, Yamada S-I. Mechanical properties of carbon fiber-reinforced aluminum alloys with whiskers and particulates of silicon-carbide. Trans JIM. 1988;29(4):314-21.
[77] Dong X, Jahanmir S, Hsu SM. Tribological characteristics of alpha-alumina at elevated temperatures. J Am Ceram Soc. 1991;74:1036-44.
[78] Parry TV, Wronski AS. The effect of hydrostatic pressure on the tensile properties of pultruded CFRP. J Mater Sci. 1985;20:2141-7.
[79] Parry TV, Wronski AS. The tensile properties of pultruded GRP tested under superposed hydrostatic pressure. J Mater Sci. 1986;21:4451-5.

[80] Sigley RH, Wronski AS, Parry TV. Tensile failure of pultruded glass–polyester composites under superimposed hydrostatic pressure. Compos Sci Technol. 1991;41:395-409.

Figures

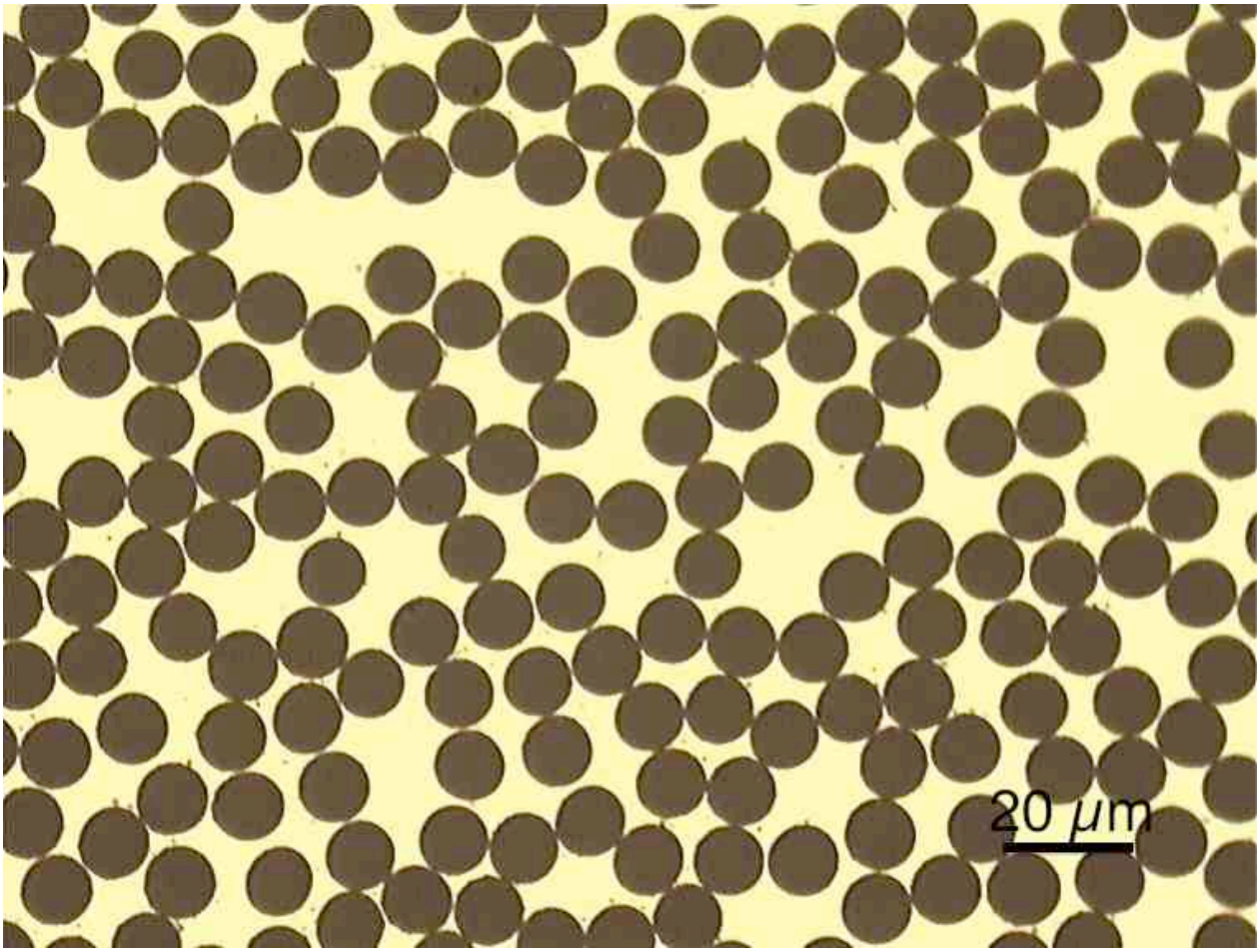

(a)

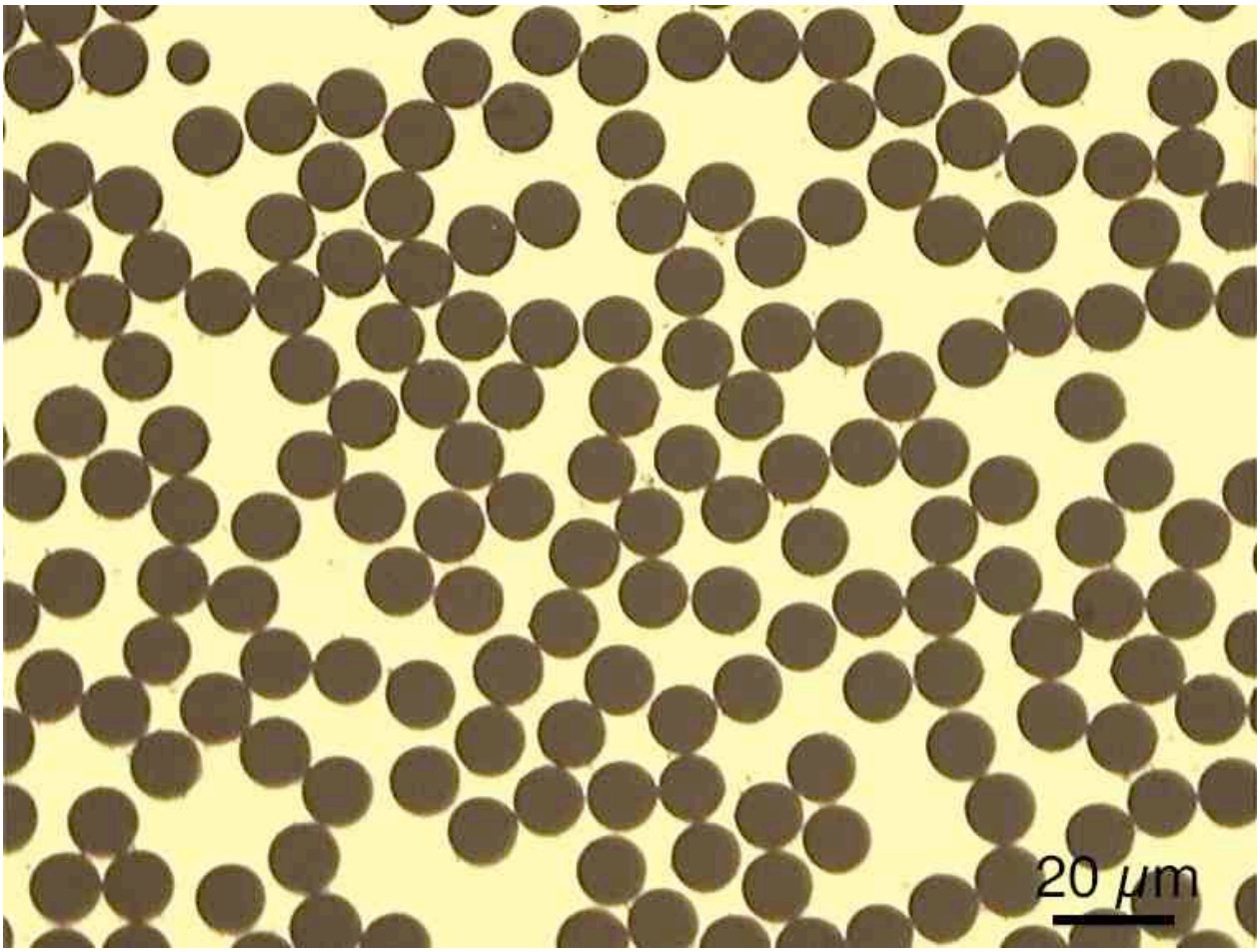

(b)

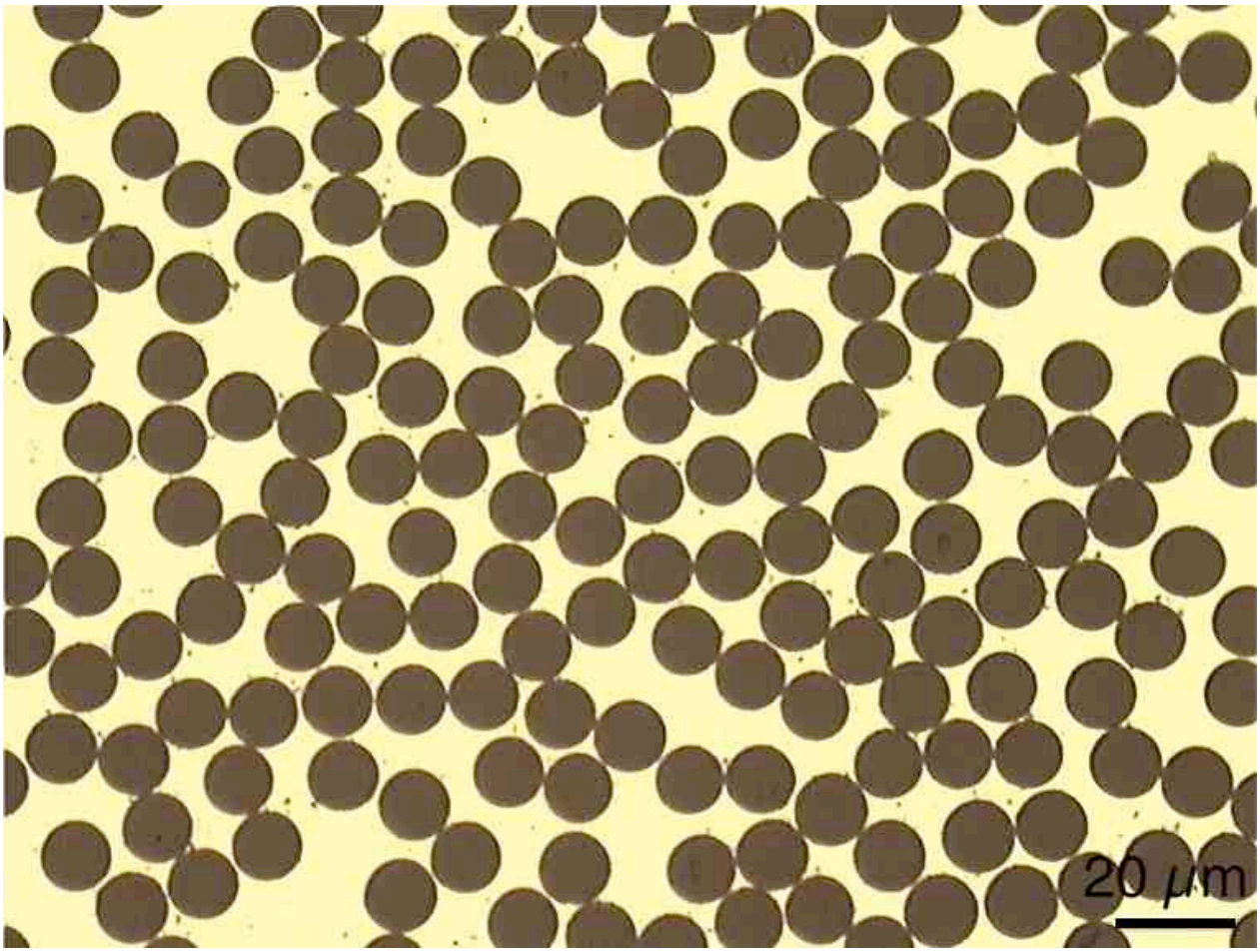

(c)

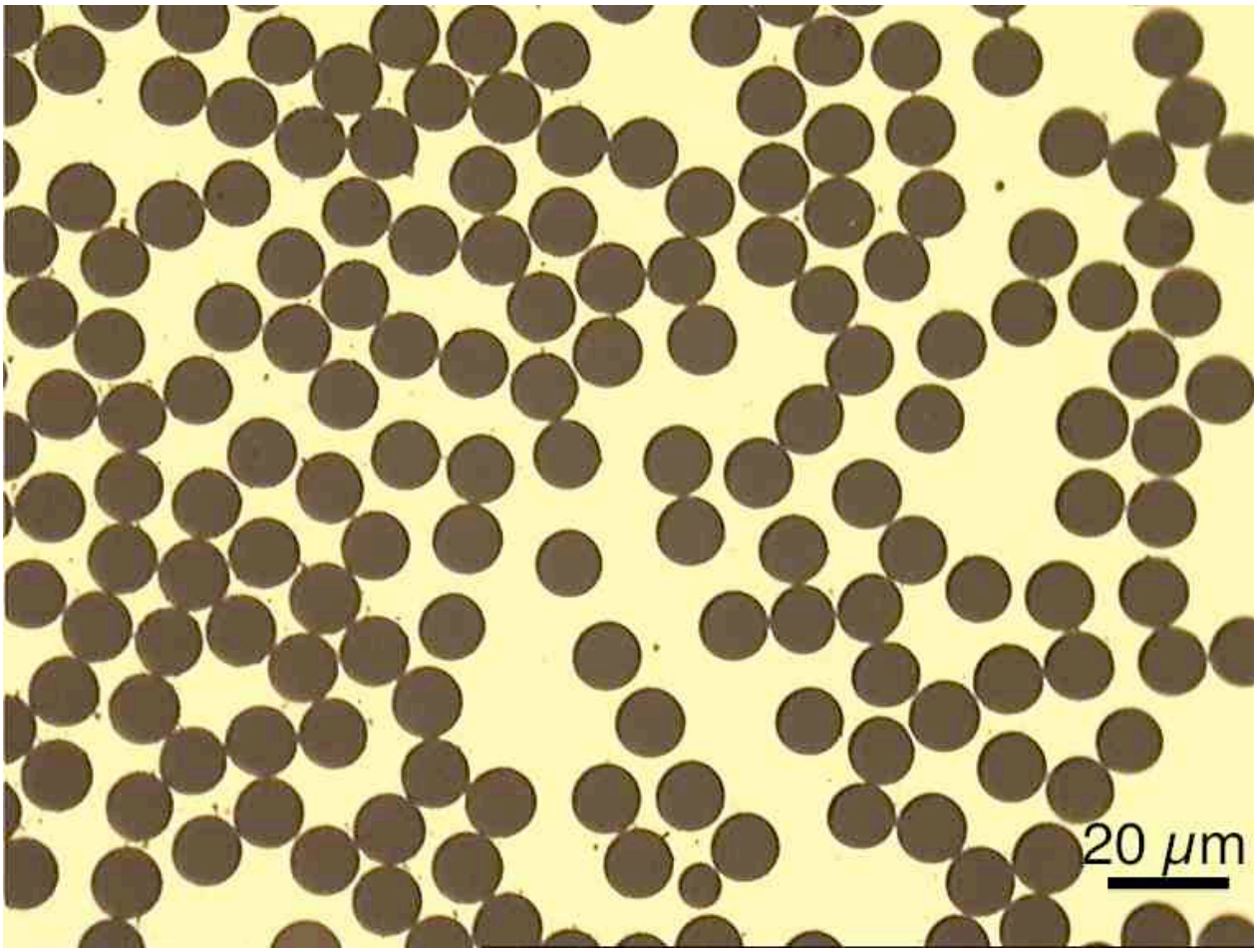

(d)

Figure 1. Micrographs of the composite wire. Corresponding volume fractions of fibre reinforcement are 60.9%, 54.7%, 59.1% and 51.9%, respectively.

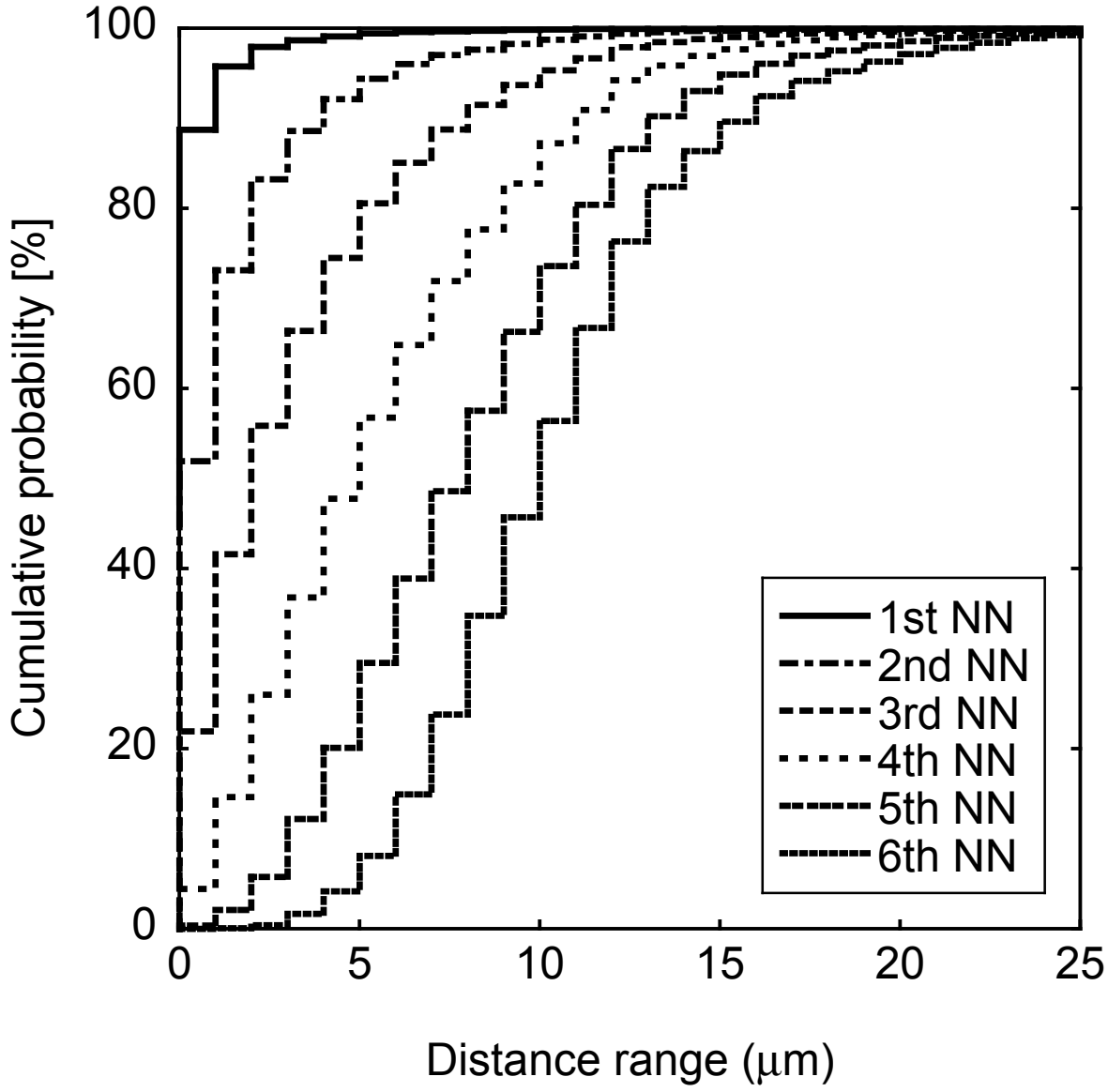

Figure 2. Distribution of neighbouring fibres. (NN = nearest neighbour)

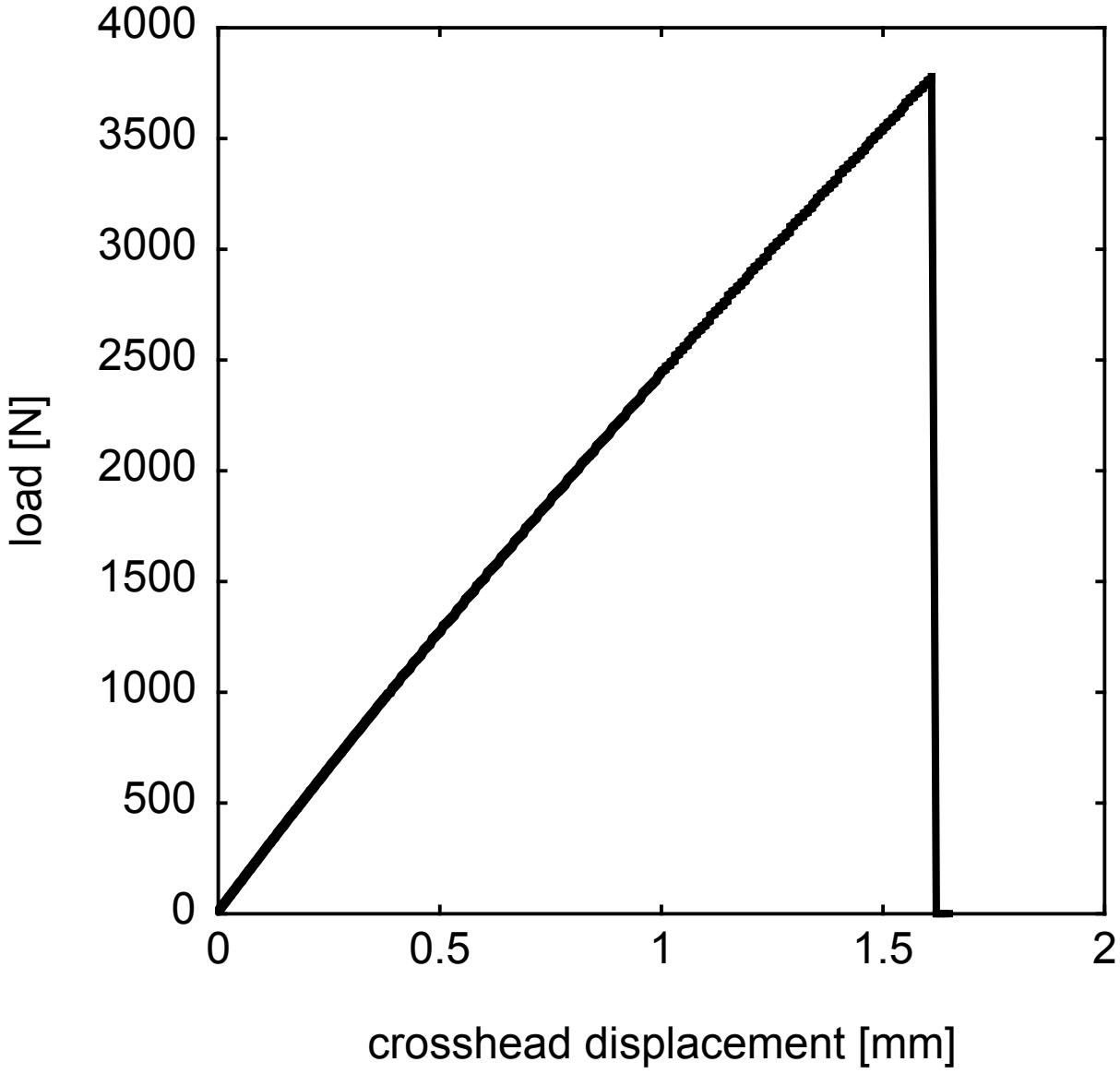

Figure 3. Typical load–displacement plot of a tensile test, here carried out at 600 °C.

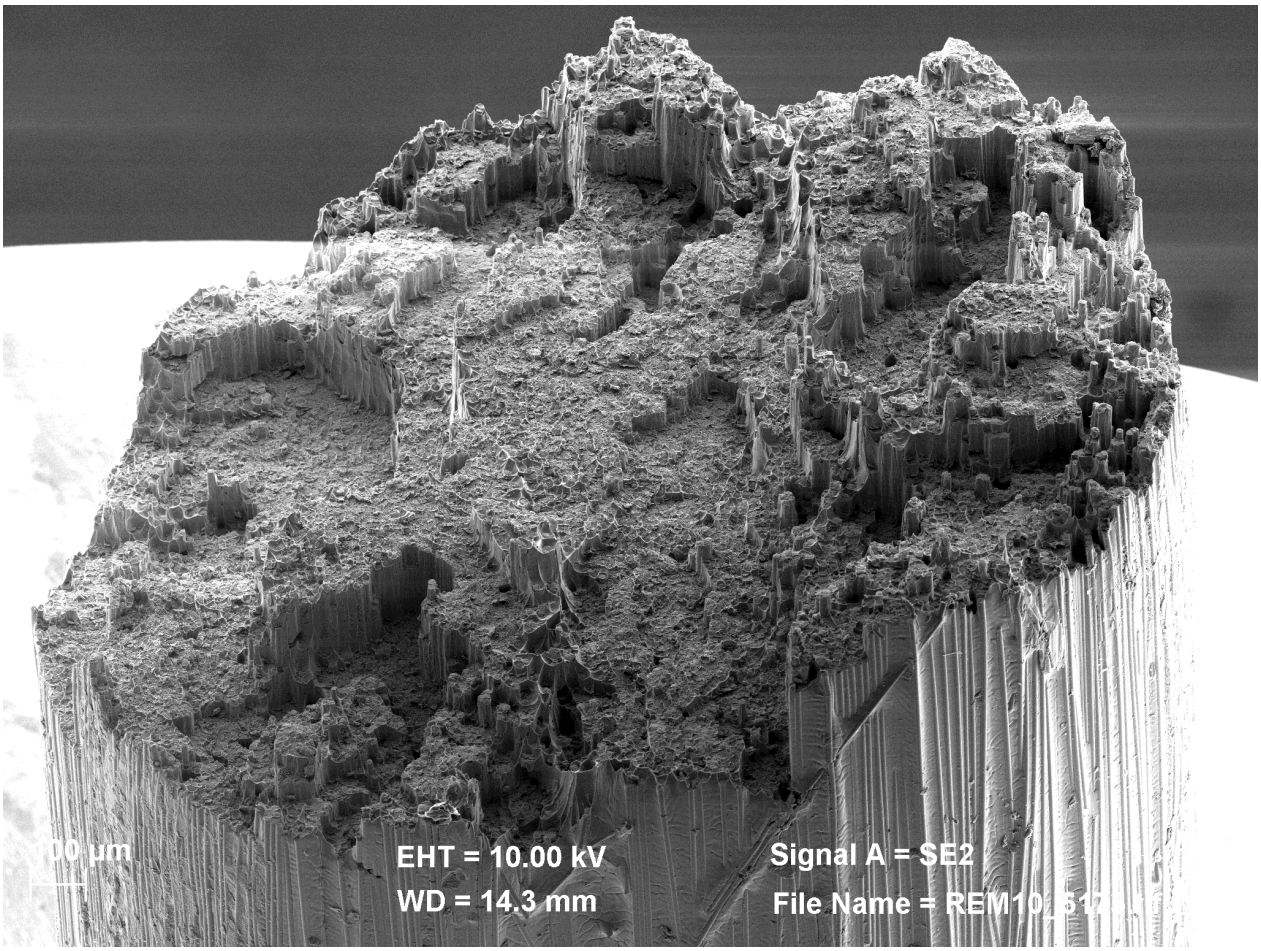

(a)

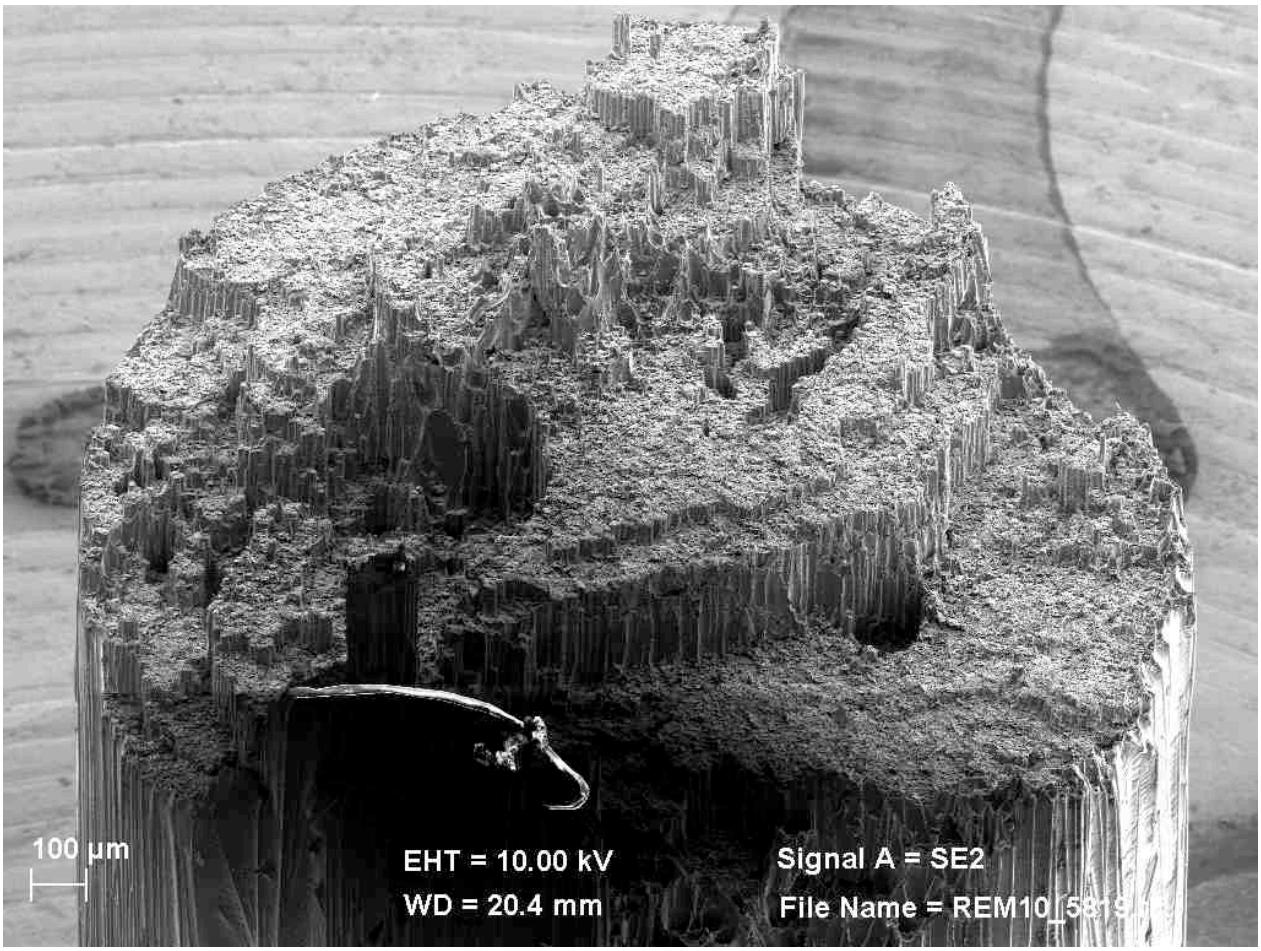

(b)

Figure 4. Fractography of composite wire (a) tested at room temperature, and (b) tested at 600 °C. Arrows indicate regions of more pronounced matrix plasticity.

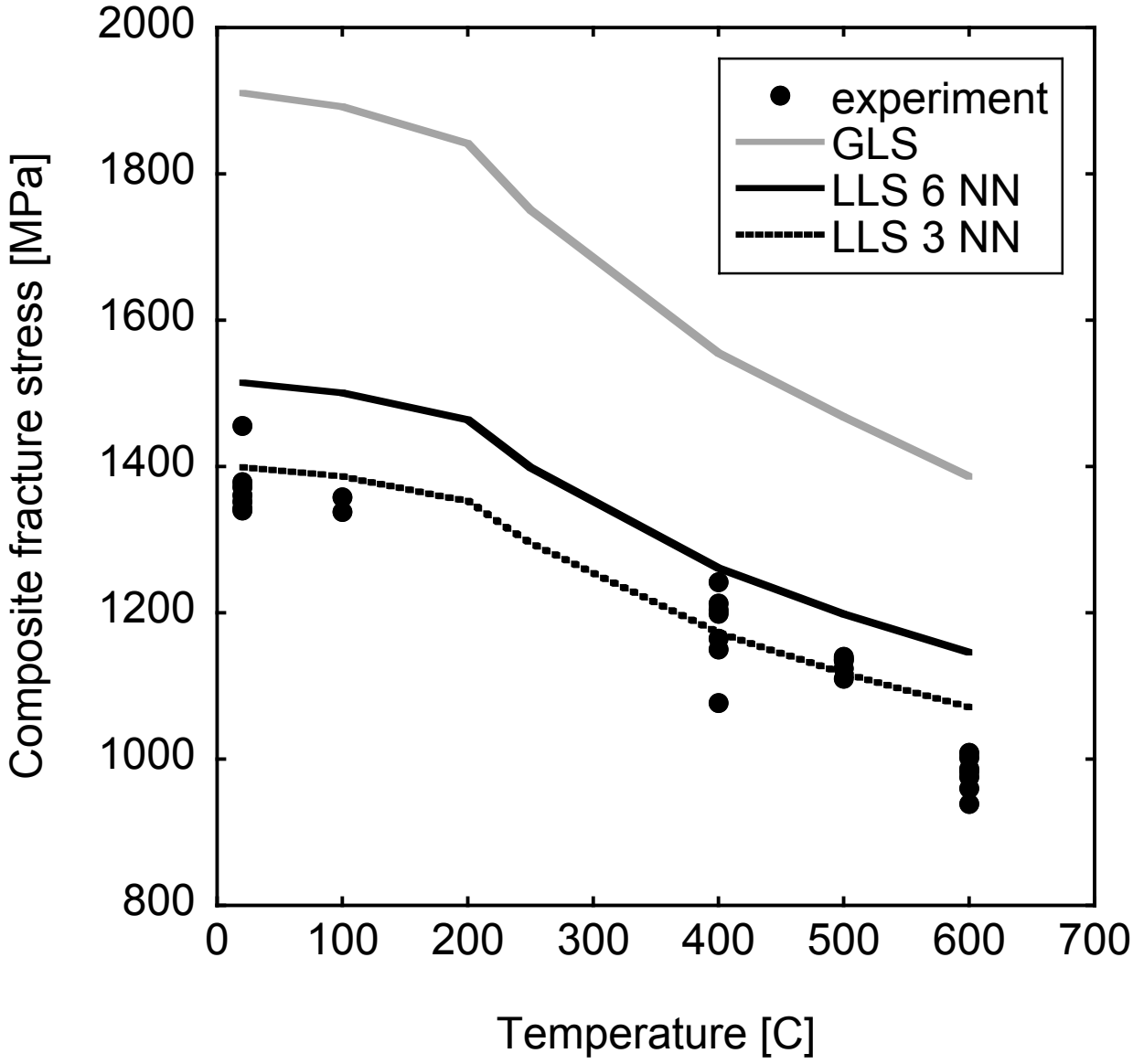

Figure 5. Experimental as well as computed values of composite strength as a function of test temperature.

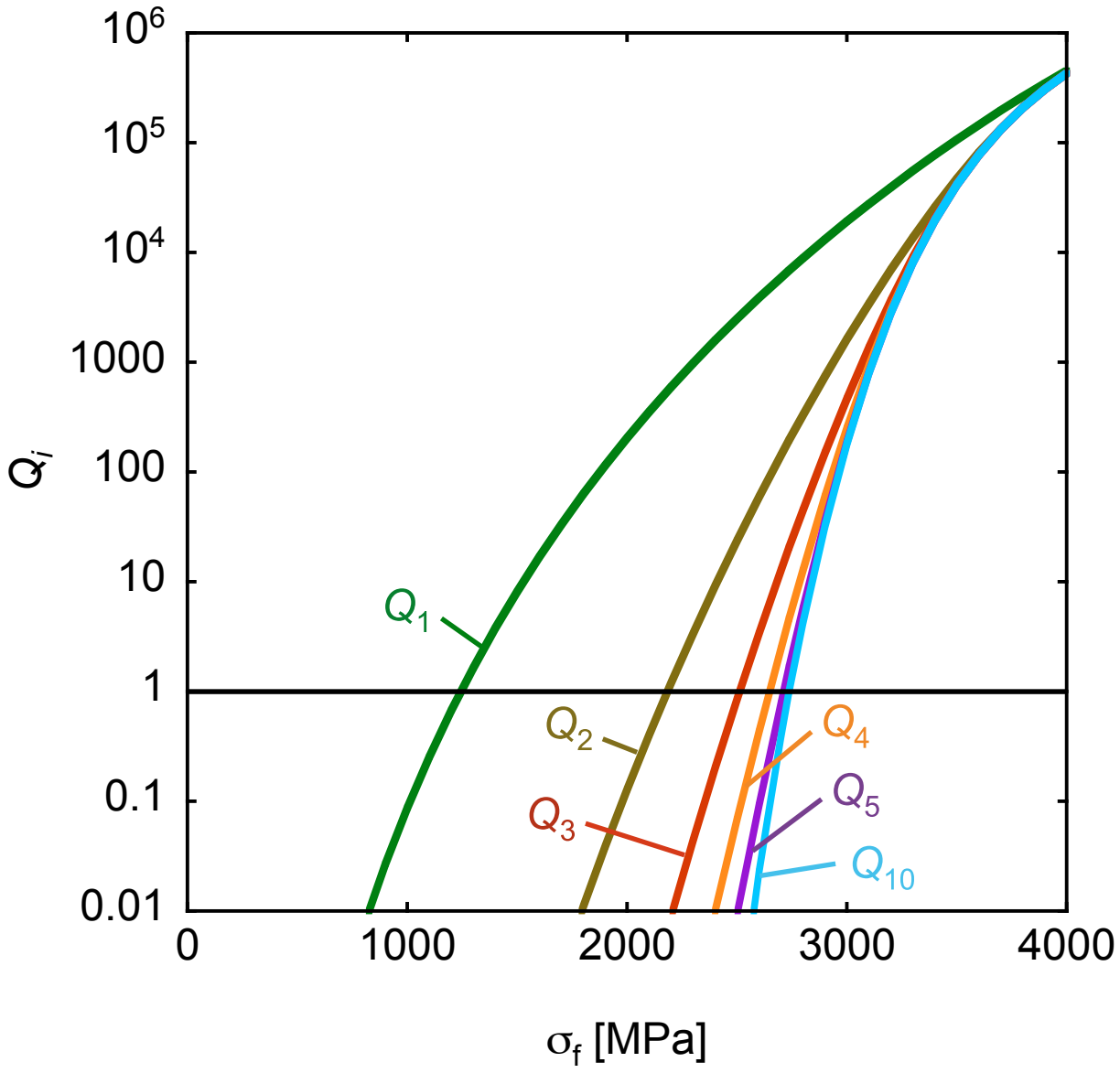
10^6
10^5
10^4
1000
100
10
1
0.1
0.01
Q_i
Q_1
Q_2
Q_3
Q_4
Q_5
Q_{10}
0
1000
2000
3000
4000
σ_f [MPa]

(a)

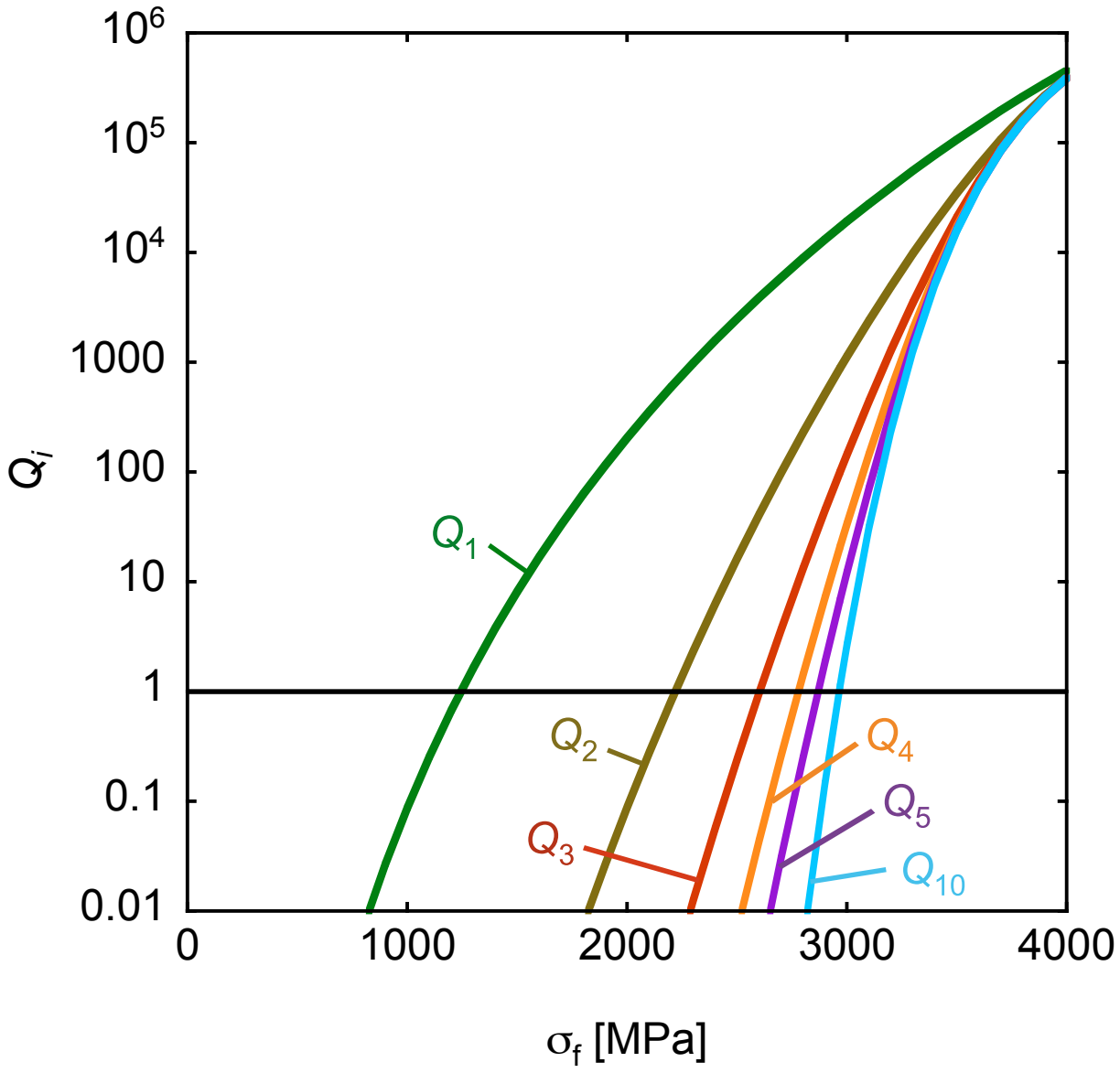

(b)

Figure 6. Evolution of Q_i for i-plets with 1, 2, 3, 4, 5 or 10 fibres, considering that each fibre has three (a) or six (b) neighbours. For i-plets with more than roughly 10 fibres, resulting Q_i curves overlap. Instability occurs when $Q_i = Q_{i+1} = 1$.

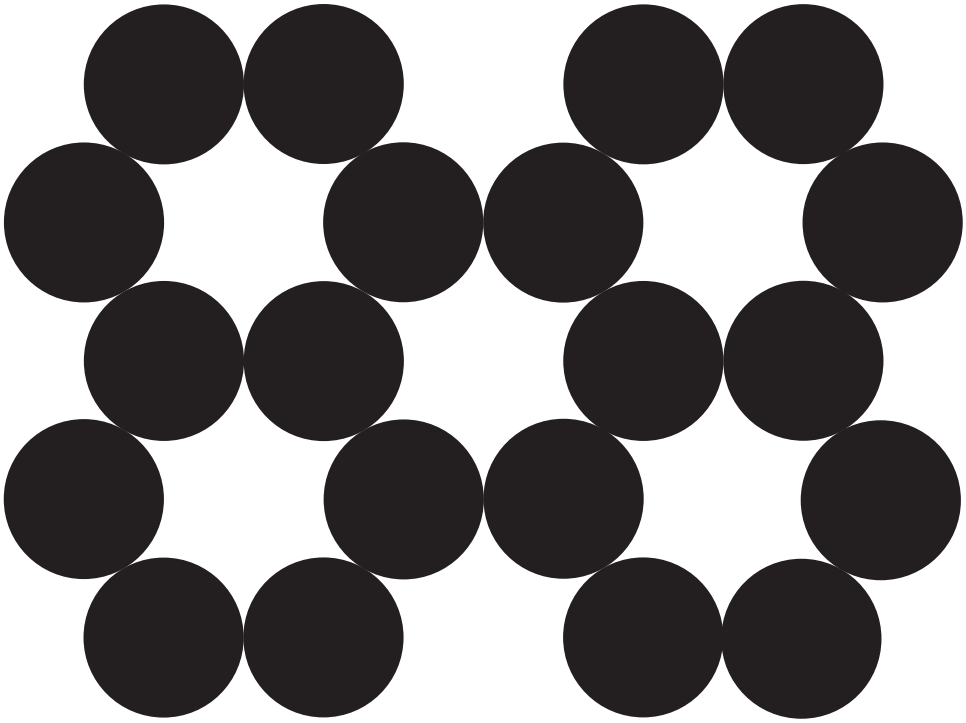

Figure 7. Idealized hexagonal-grid fibre arrangement giving each fibre three direct neighbours instead of six.

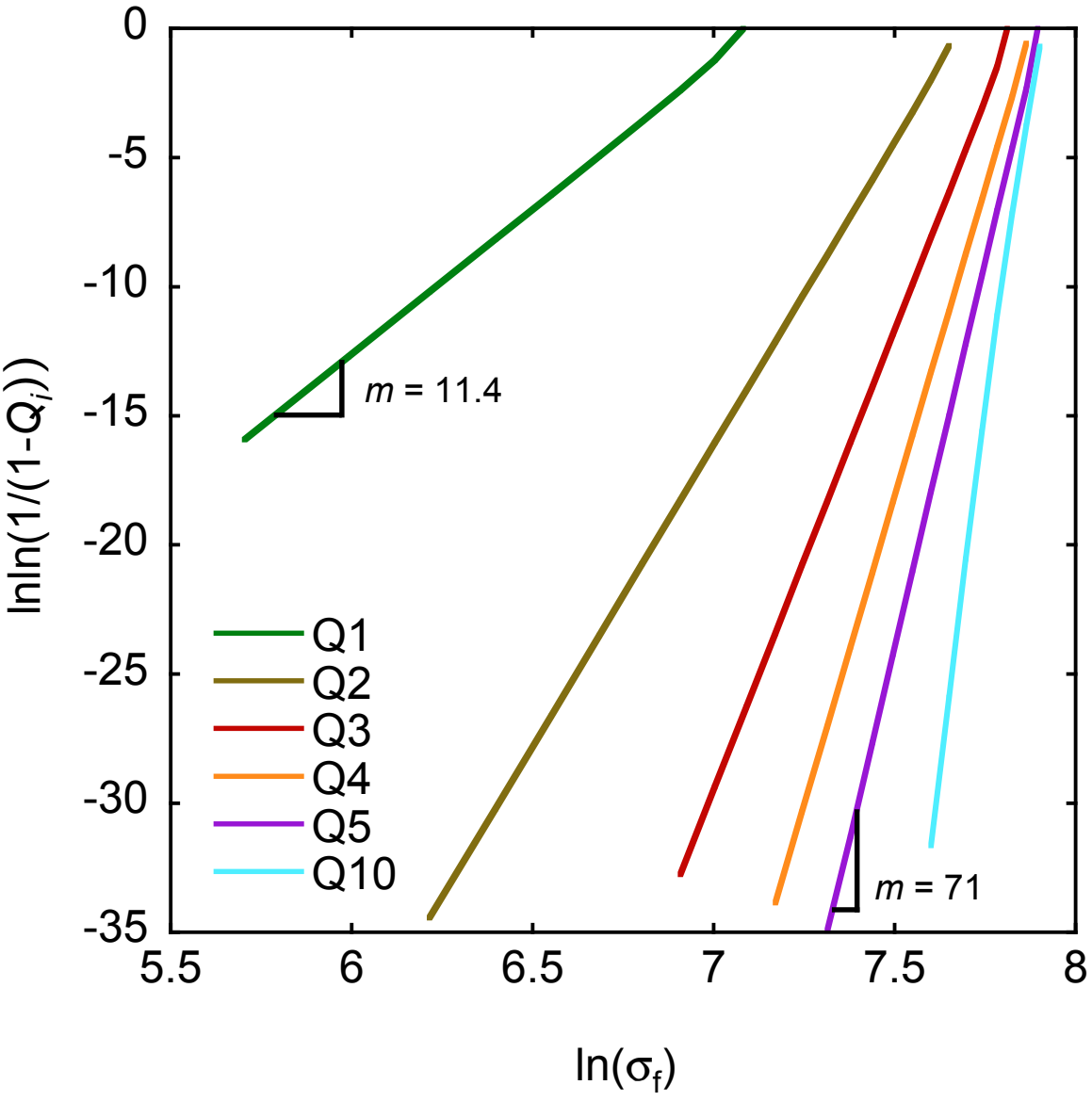

Figure 8. Double logarithmic plot of the lower end of Fig. 6a.